Corrosion Science 185 (2021) 109435

Contents lists available at ScienceDirect

Corrosion Science

journal homepage: www.elsevier.com/locate/corsci

Depth profiling approach to evaluate the influence of hot stamping on the local electrochemical behaviour and galvanic series of hot-dip Al-Si coating on 22MnB5 steel

Camila Pucci Couto [a,b,c,*], Francesco Andreatta [d], Alex Lanzutti [d], Isolda Costa [a], Zehbour Panossian [c], Iris De Graeve [b], Herman Terryn [b], Jesualdo Luiz Rossi [a], Reynier I. Revilla [b]

[a] Nuclear and Energy Research Institute, Materials Science and Technology Centre, Av. Prof. Lineu Prestes 2242, 05508-000, São Paulo, Brazil
[b] Vrije Universiteit Brussel, Department of Chemistry and Materials, Research Group Electrochemical and Surface Engineering, Pleinlaan 2, 1050, Brussels, Belgium
[c] Institute for Technological Research, Laboratory for Corrosion and Protection, Av. Prof. Almeida Prado 532, 05508-901, São Paulo, Brazil
[d] University of Udine, Polytechnic Department of Engineering and Architecture, Via del Cotonificio 108, 33100, Udine, Italy

ARTICLE INFO

Keywords:
Hot-Stamping
Al-Si coating
Press-hardened steel
GDOES
Electrochemical micro-cell

ABSTRACT

The influence of hot-stamping process on the corrosion properties of Al-Si coating on 22MnB5 steel was locally evaluated using a depth profiling approach combining GDOES and electrochemical micro cell. The results highlight the complexity of the system and the high dependence of the local galvanic series on the hot-stamping process. Due to iron diffusion from the steel substrate into the coating, the Al-rich layers presented active behaviour, whereas the initial coating condition showed a passive behaviour. Conversely, Fe/Si-rich sublayers acted as protective barrier for the steel substrate, as they show passive behaviour with nobler corrosion potentials and lower current densities.

1. Introduction

The replacement of conventional steel grades by ultra-high strength steels (UHSS) in vehicle structures has led to mass reduction and, consequently, reduced fuel consumption. Moreover, the use of these UHSS grades allows safety / crashworthiness improvement. These key factors are achieved due to higher tensile strength and thinner thickness than the conventional steels [1–6]. However, due to their high tensile strength, they are more prone to the springback effect. The springback influences mainly the final shape of the component due to the residual stress when the component is cold worked at room temperature [7,8]. As an alternative to the cold-forming process, the hot stamping has been applied on a large scale to produce UHSS components. The industrial method consists of heating a steel blank at total austenitization temperatures and then transferring it from the furnace to the press tool for simultaneous quenching and forming of the material. The hot-stamping conditions may vary according to the manufacturer [1,6,9–13]. At the end of the process, the steel is known as press-hardened steel (PHS) [8].

Structural vehicle components of boron-manganese steel have been widely produced by means of the hot-stamping process, due to this steel's high hardenability and quenchability, which are inherent to the steel-grade chemical composition, allowing the fully martensitic transformation by the end of the thermo-mechanical process [1,12]. Due to the high temperatures used in the hot stamping process, the formation of oxide on the surface and decarburization of the steel by the contact of atmospheric air can occur during the transfer of the blank from the furnace to the press. The oxide layer formed has high hardness that results in premature wear of stamping dies; whereas decarburization directly affects the final properties of the part, since carbon in combination with atmospheric oxygen ceases to exercise its steel hardening function [1,4,9,12,14–16].

Different metallic coating systems have been developed and evaluated specifically for hot-stamping applications as Fan et al. [17] have reviewed. The main required properties for a coating, developed specifically for hot stamping, include sufficient oxidation resistance, good formability at room and high temperatures, good corrosion resistance, presenting barrier and cathodic protection mechanisms, paint adhesion and weldability [17,18]. Among the metallic coating systems, Al- and Zn-based coatings have been the most evaluated. These systems are known for forming thermodynamically stable oxides which play a role of

* Corresponding author at: Nuclear and Energy Research Institute, Materials Science and Technology Centre, Av. Prof. Lineu Prestes 2242, 05508-000, São Paulo, Brazil.
E-mail addresses: camila.puccicouto@usp.br, Camila.Pucci.Couto@vub.be (C.P. Couto).

https://doi.org/10.1016/j.corsci.2021.109435
Received 27 November 2020; Received in revised form 19 March 2021; Accepted 1 April 2021
Available online 2 April 2021

barrier protection [3]. However, the most applied system has been the hot-dip aluminium-silicon (Al-Si) with a near eutectic composition (7 % to 11 % Si in mass fraction) [1–4].

The hot-dip Al-Si has been extensively investigated in terms of structure morphology and corrosion properties [19–22]. The coating consists of different sublayers: the aluminium coating matrix and the interdiffusion layers. The aluminium matrix is thicker than the interdiffusion layers and contains cathodic Al-Fe-Si precipitates. The interdiffusion part of the coating is composed of an upper and a lower interdiffusion layer (UIDL and LIDL, respectively). The LIDL is known as a hard and brittle Al-Fe alloy phase, often reported as η - Al_5 Fe_2, adjacent to the steel substrate. The silicon addition suppresses the growth of the LIDL and promotes a smoother interface between the steel and the coating. The UIDL is characterised as a mixture of θ-$Al_{13}Fe_4$ and τ_5-Al_7Fe_2Si, more ductile than the LIDL [19,20,22]. The complex structure of such Al-Si coatings changes completely due to the hot-stamping process. The coating becomes much more complex because of the iron diffusion into the coating. The sublayers formed are either enriched in aluminium or iron [2,3,14]. Silicon is present in solid solution and at high concentration in the iron-rich sublayers [2,3,23]. Moreover, silicon plays a role of hindering the growth of the brittle aluminium-rich layers. The aluminium-rich sublayers show low fracture toughness and hardness of 900–1150 HV·0.05 whereas the iron-rich sublayers have been reported to present high fracture toughness and hardness of 300–600 HV·0.05 [2]. Windmann et al. [2] have shown that the volume fraction of the iron-rich phases increases (AlFe) while that of the aluminium-rich phases (Al_5Fe_2) decreases when longer soaking time at high temperatures are set during hot stamping. After the hot stamping, the interface between the coating and the steel substrate consists of a single interdiffusion layer (IDL) enriched in iron and little amount of aluminium and silicon. The presence of voids, often seen in the IDL, is a consequence of the fast diffusion; the volume ratio increases with time and temperature. The presence of voids in the IDL promotes the initiation of cracks, being detrimental to the general coating properties [2,24,25].

On the other hand, the corrosion resistance of coated PHS is still a subject of investigation. Most of the published corrosion studies have used either standard electrochemical measurements or accelerated corrosion tests to evaluate the corrosion properties of PHS [4,9,13,26]. However, these methods only show the global behaviour of the system and they do not give any insights concerning the local electrochemical behaviour of the different sublayers of the coatings. There is a need for a more local investigation of these systems due to the high complexity of these multi-layered systems, highlighted by the different compositions of the sublayers and the presence of defects (micro cracks and voids). For this reason, a detailed approach based on local electrochemical techniques is suggested. Studying the electrochemical behaviour of the different sublayers in the coating is of paramount importance since in the case of scratches or damage to the coatings, the steel substrate may become exposed. This also relates to the exposure of cut-edge and issues related to joining-processes, such as welding and adhesives.

Local electrochemical techniques have been used to investigate the activity of micro-galvanic cells formed in different systems, such as: passive alloys, cut-edge corrosion, influence of intermetallics, effect of deformation and also on the galvanic coupling steels coated with hot-dip Al-Si [19,20,27–30]. These techniques can be divided into two main groups: either based on scanning or on small-area electrode methods [30–32]. The effect of the hot stamping on the electrochemical behaviour of 22MnB5 steel coated with hot-dip Al-Si (Si 10 % in mass fraction) was evaluated by means of scanning Kelvin probe force microscopy (SKPFM). It was shown that the thermo-mechanical process has a great influence on the driving force for cathodic protection, since the difference of (Volta) potential between the steel substrate and the coating layer decreases [23]. Although, this technique provides insights into the behaviour of the galvanic coupling (steel / coating) in its passive state, considering the absence of an electrolyte, the technique does not provide information about the local current flow, an important parameter to determine the kinetics of the corrosion process. This is actually the major drawback of the scanning techniques which do not allow direct corrosion current measurement [31–33]. Conversely, with the small-area electrode techniques, the measurement of current is directly possible. These techniques are based on the principle of decreasing the area to be analysed in a range of micrometres and still conduct the standard electrochemical measurements [28,30,31,34,35]. The use of the electrochemical micro cell was first introduced by Suter[1] et al. [32].

In the present work, the influence of hot stamping on the coating corrosion properties, considering each sublayer, was evaluated using a depth profile approach combined with localised electrochemical measurements. Layer by layer of the coating, either before or after hot stamping, was exposed by means of glow discharge optical emission spectroscopy (GDOES), after which, the electrochemical activity of each layer was evaluated using an electrochemical micro cell. This approach has been chosen to provide a better insight of thermodynamic and kinetic parameters of the localised corrosion mechanism induced by the galvanic couplings between the different layers of the coating and the steel substrate.

2. Experimental

2.1. Samples

Industrial samples of 22MnB5 steel coated with hot-dip Al-Si (Si 10 % in mass fraction) were used. The samples were divided in two different conditions: before and after hot stamping. The samples before hot stamping are designated as “as-received Al-Si” (AR). After the thermo-mechanical process, the samples are named as “press-hardened steel” (PHS). The AR specimen was cut-off from the coated steel blanks and the PHS sample was cut-off from a door beam structural vehicle component, provided by a carmaker. Table 1 shows the nominal chemical composition of the 22MnB5 in terms of maximum % in mass fraction, according to the steelmaker specifications [36].

According to the specifications [37], the coating applied to the AR samples is the AS150 which shows thickness of 25 μm per side and mass of 150 g m^{-2} double-sided. On the other hand, the blanks designated for the hot stamping were first coated with the AS80 coating. This coating has thickness of 14 μm per side and mass of 80 g m^{-2} double-sided. The blanks coated with AS80 were then submitted to the hot-stamping process.

2.2. Coating characterisation

The cross sections of both sample conditions were characterised by means of field emission-scanning electron microscopy (FE-SEM) and the images were obtained in the backscattering mode. The samples were prepared according to standard metallographic procedures: hot mounting in carbon resin, grinding and polishing. Fig. 1 shows the cross-section images of the AR (a) and PHS (b) samples after the metallographic procedures for further FE-SEM analyses. The equipment was set to operate with 15 kV acceleration voltage, 12 pA probe current and a working distance of approximately 10 mm. The semi-quantitative elemental analyses were undertaken by means of energy dispersive X-ray spectroscopy (EDS). The EDS analyses were performed in two different ways: local identification (point ID) and mapping.

2.3. Depth profile local electrochemical measurements

In-depth composition profiles were recorded by GDOES. The instrument was equipped with a standard 4 mm diameter anode, a

[1] This paper is dedicated to the memory of Dr. sc. techn. Thomas Suter, who passed away on April 20, 2020.

Table 1
Nominal chemical composition of 22MnB5 steel in terms of maximum % in mass fraction.

Grade	C	Si	Mn	P	S	Al	B	Ti + Nb	Cr + Mo
22MnB5	0.25	0.4	1.4	0.03	0.01	0.1	0.005	0.12	1

Source: ArcelorMittal [36].

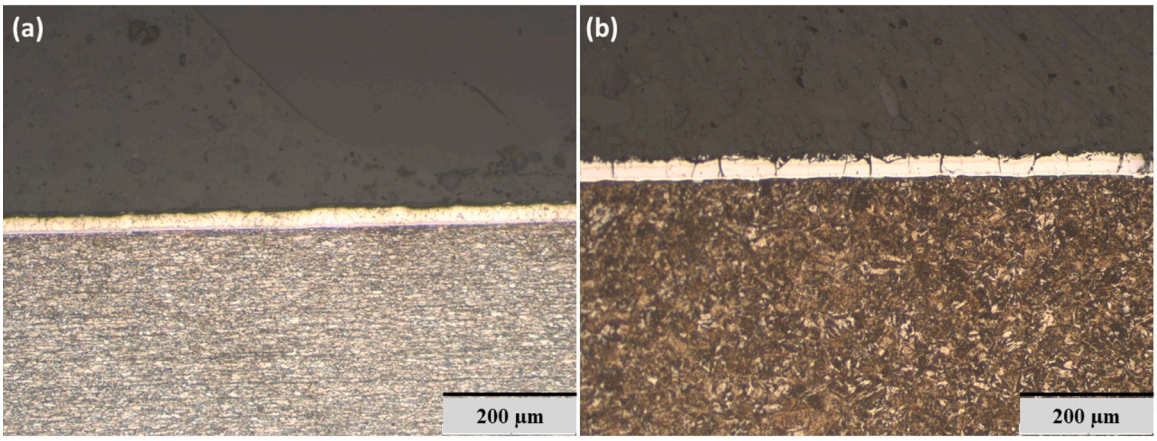

Fig. 1. optical microscopic images showing the conditions of the coating layer of (a) AR and (b) PHS, just after the metallographic procedures.

polychromator with 28 acquisition channels, an RF-generator (13.6 MHz) and a Quantum XP software. The analysis conditions were: argonium pressure of 620 Pa and applied power of 35 W. The instrument was equipped with a 0.5 m polychromator with nitrogen purged optical path. The calibration was performed with 28 samples selected among setting up samples (SUS) and certified reference material (CRM) which were ground and polished before use. The different sputtering times to reach the different sublayers have been chosen based on the complete depth profile for each sample condition. The sputtering times established for the AR condition were: 50 s, 100 s, 250 s and 350 s. These sputtering times represent a depth of approximately 2.5 µm, 7.5 µm, 12.5 µm and 17.5 µm, respectively. Moreover, a longer sputtering was performed in order to reach the steel substrate. Otherwise, the sputtering times established for the PHS samples were: 70 s, 140 s, 280 s and 400 s; which represent a depth close to 3 µm, 7 µm, 15 µm and 21 µm respectively. Additional sputtering of 500 s and 1000s to reach the steel substrate were also carried out. The schematic experimental approach of the depth-profile local electrochemical measurements is shown in Fig. 2. Nevertheless, it is important to mention that it was used a different sample for each crater made.

Localised anodic potentiodynamic polarisation measurements were carried out in the different craters obtained by GDOES for the AR and PHS samples using the electrochemical micro-cell technique. A capillary glass with an internal diameter of 800 µm was selected to perform the measurements. This corresponds to an area of the working electrode of 5×10^{-3} cm^2. This capillary size was chosen because it is large enough to obtain results, which are less influenced by changing the amount of precipitates and / or of defects in the area of investigation (as seen in Fig. 1), but small enough to have the ability to perform 3–4 measurements per crater [30]. The measurements were carried out with a current resolution in the order of 10 fA. The micro cell presented a three-electrode configuration: the sample under investigation as working electrode, a Pt counter electrode and a Ag|AgCl|3 mol·L^{-1} KCl reference electrode. The potentiodynamic polarisations were started

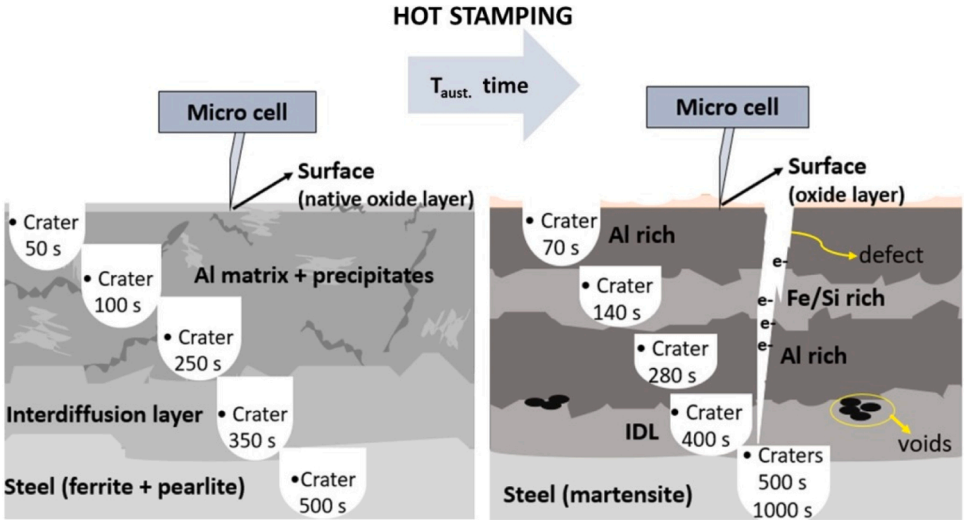

Fig. 2. Schematic of the experimental approach used during the depth-profile local electrochemical measurements, showing the influence of the hot-stamping process on the 22MnB5 steel coated with hot-dip Al-Si.

after a short stabilization time without recording the open circuit potential (*OCP*). This was necessary to avoid leakage of solution from the micro capillary during the potentiodynamic polarisation tests [30]. The scan started at −200 mV vs *OCP* (open circuit potential), with scan rate of 1 $mV{\cdot}s^{-1}$ in 0.1 $mol{\cdot}L^{-1}$ NaCl solution. For each layer, at least three polarisation curves were recorded. Additionally, localised anodic potentiodynamic polarisations were recorded on the non-sputtered top surfaces of AR and PHS samples. Finally, to confirm the position of the craters made by GDOES, they were also sectioned after the potentiodynamic polarisation and analysed by SEM.

3. Results

3.1. Coating characterisation

The cross-section morphology of the as-received 22MnB5 steel coated with hot-dip Al-Si (10 % Si in mass fraction) and the EDS analyses are shown in Fig. 3. The coating comprises of two main layers (1 and 2) and a thin and discontinuous layer adjacent to the steel substrate (3). The first layer is often called the outer layer or free aluminium layer (FL) due to the high amount of aluminium present (Fig. 3 (c) - spectrum 1) [19,20]. In addition, two different precipitates are seen in this first outer layer. According to the EDS mappings in Fig. 3 (c), the precipitates consist of either Si or Fe-Al-Si. The second layer is known as interdiffusion layer (IDL); the amount of iron increases in this layer due to the chemical diffusion which takes place during the hot-dipping process [19–23]. Moreover, the amount of silicon in the IDL is also near to the molten bath chemical composition (Fig. 3 (c) - spectrum 2). Nevertheless, it has been reported that the IDL in hot-dip aluminized steels is actually composed of two sub layers: the upper and the lower interdiffusion layer (UIDL and LIDL, respectively). This is clearly seen in the inset image in Fig. 3 (a), highlighting the layer 2 in which the two sublayers are present. The LIDL is characterised as the discontinuous thin layer (3) adjacent to the steel substrate; it comprises higher iron and lower silicon content in comparison with the UIDL (Fig. 3 (c) - spectrum 3).

From Fig. 3 (a), a planar interface is observed between the steel substrate and the coating layer; it has been attributed to the effect of silicon addition. Moreover, silicon has an influence on the thickness of the LIDL which is a hard and brittle phase; the cracks seen in the interdiffusion layer were probably originated in the LIDL. The proposed mechanism, suggested in the literature, is that silicon occupies the vacancies in the lattice of the corresponding phase for the LIDL, suppressing its growth and promoting the growth of the UIDL which is a ductile phase [2,3,22,38]. The exact stoichiometry of the two different phases formed in the IDL after hot-dipping process is still a subject of many controversies in the literature. These phase formation and growth are strongly dependent on the molten bath chemical composition and on the hot-dip process parameters [22,38,39].

Fig. 4 (a) shows the effect of hot stamping on the coating morphology. After the thermo-mechanical process, a more complex multi-layered structure is formed, mostly related to the diffusion of iron from the steel substrate into the coating layer [1–3,6,12,17,18]. The first highlight is related to the coating thickness which is higher than the specified one for the AS80 coating. The PHS condition has a coating layer around 25 μm thick. This increment is related to the diffusion of iron from the steel substrate towards the coating layer [2,3,17,18]. The coating on the PHS sample can be characterised by six different sublayers. Nevertheless, according to the semi-quantitative analyses shown in Fig. 4 (b), layers 1 and 3 have similar composition, being enriched in aluminium and designated as Al-rich phases. The layers 2, 4 and 5 also show similarity in their chemical compositions being characterised as Fe/Si-rich sub layers, based on the spectra shown in Fig. 4 (b) and also the EDS mappings shown in Fig. 4 (c). As seen in Fig. 4 (a) the sublayers 2 and 5 are continuous, except for the presence of damages often seen in PHS (see Fig. 1 (b)), such as cracks, which may cause their discontinuity. On the other hand, the sublayer 4 is discontinuous and often seen as islands morphology, similar to the small precipitates indicated by arrows as number 7. Fan et al. [18] have shown that changing the process parameters, such as austenitisation time, it promotes the formation of sublayers initially present as islands of precipitates.

The IDL (Fig. 4 (a) - number 6) adjacent to the steel substrate is mainly composed of iron and little amounts of aluminium and silicon. Although, the spectrum number 6 in Fig. 3 (b) shows little amounts of

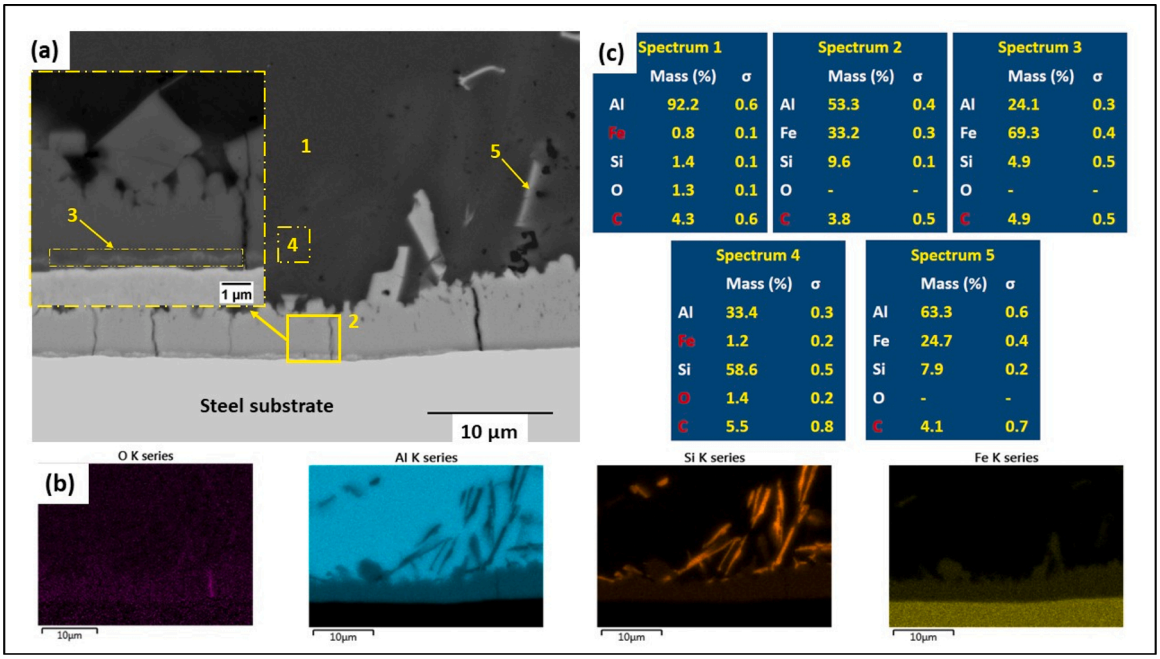

Fig. 3. Cross section morphology of as-received 22MnB5 steel coated with hot-dip Al-Si (10 % Si in mass fraction): (a) scanning backscattered image showing the main different constituents in the coating layer and an inset image highlighting the interface between coating layer and steel substrate; (b) EDS elemental mapping for O, Al, Si and Fe; (c) EDS point ID representing the semi-quantitative composition of the areas highlighted in (a).

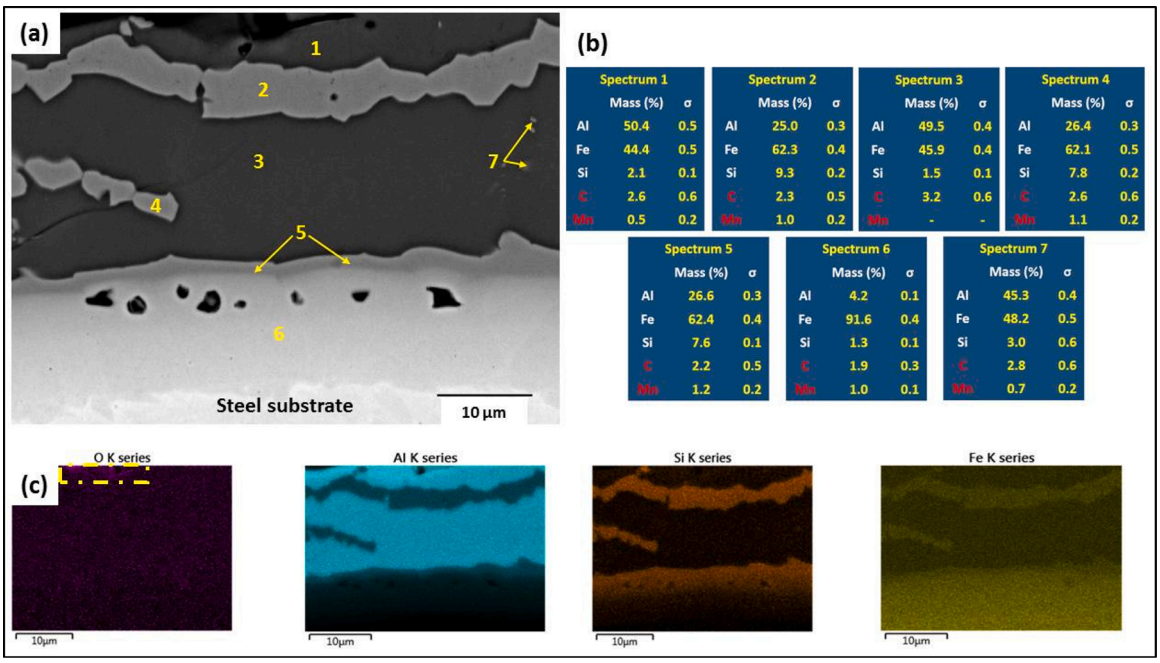

Fig. 4. Cross section morphology of press-hardened 22MnB5 steel coated with hot-dip Al-Si (10 % Si in mass fraction): (a) scanning backscattered image showing the main different constituents in the coating layer; (b) EDS point ID representing the semi-quantitative composition of the highlighted areas in (a); (c) EDS elemental mapping for O, Al, Si and Fe.

aluminium and silicon, the EDS mapping in Fig. 3 (c) shows that mainly the silicon content decreases gradually throughout the IDL. Moreover, voids are seen mainly in the IDL, indicating different diffusivity among the chemical elements [2]. It is important to point out that after hot stamping the Si and Fe-Al-Si precipitates are no longer seen in the coating. After the thermo-mechanical process, silicon is present in solid solution and its concentration varies among the sublayers [2,3]. However, a high silicon content is seen in the Fe-rich layers: (Fig. 4 (a) - layers 2, 4 and 5). According to the literature, the number of sublayers as well as their chemical composition is strongly dependent on the austenitization conditions during hot stamping (e.g. soaking temperature and time) [3,38]. In both sample conditions, AR and PHS, the EDS spectra (point ID) show the presence of carbon and manganese. Manganese was present in the bulk composition of the steel. It is possible that it also diffused during hot stamping, while the carbon is a contamination arising from the samples' preparation. Moreover, oxygen is seen in the EDS mappings for both conditions. It suggests the presence of an oxide layer at the outer surface which may play an important role on the corrosion mechanism. However, as seen at the top of the EDS oxygen map for PHS (yellow dashed line in Fig. 4 (c)), the concentration of oxygen is higher suggesting that the oxide layer formed on the outer surface after hot stamping is thicker than for as-received specimens, as also shown in previous studies [2,3,18]. This thicker oxide layer may play an important role in the corrosion behaviour of the PHS samples.

The complexity of the Al-Si coating system, either before or after hot stamping, is well highlighted from the cross-section characterisations in Figs. 3 and 4. Considering the different phases present in both sample conditions, they will contribute to the corrosion process based on the different galvanic couples which are formed either among the different sublayers or between the coating and the steel substrate. For these reasons, the electrochemical behaviour of both systems, before and after hot stamping, was investigated on a localised scale.

3.2. GDOES depth profile

GDOES is used here as a tool for sample preparation for electrochemical depth profiling with the micro cell, but of course it also gives valuable compositional data that shows the diffusion profile of the

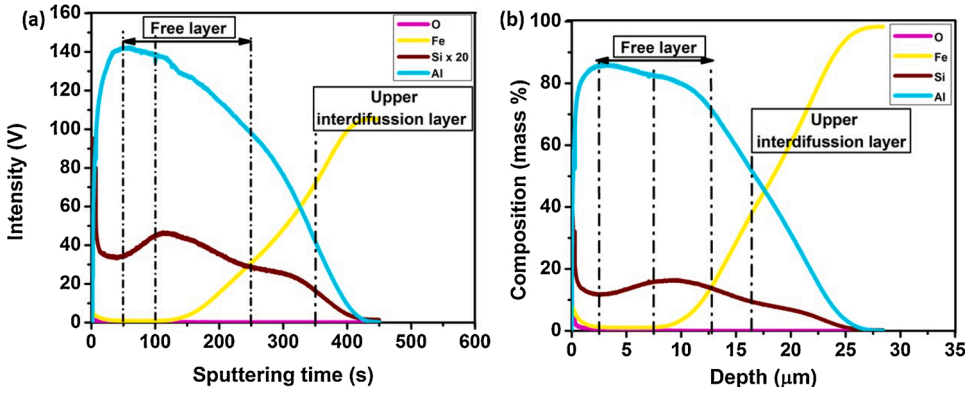

Fig. 5. GDOES profiles for as-received 22MnB5 steel coated with hot-dip Al-Si. (a) sputtering time profile showing by dashed lines the craters obtained after 50 s, 100 s, 250 s and 350 s of sputtering; (b) depth profile showing the craters obtained as a function of their depth and elemental chemical composition for Al, Si, Fe and O.

elements from the coating layer towards the steel substrate and vice-versa. The GDOES depth profiles for the AR sample are shown in Fig. 5. From the depth profile (Fig. 5 (b)), it is seen that the thickness of the coating layer is about 25 μm, mainly composed of aluminium, in agreement with the results shown in Fig. 3. The amount of aluminium decreases towards the steel substrate, while the iron content increases from the depth of 10 μm. The diffusion interface for the Al-Fe diffusion couple is approximately at 17 μm. At this depth, the composition of both aluminium and iron is about 45 % in mass fraction. The silicon profile shows that it is distributed in the whole coating layer. The distribution of silicon seen in the GDOES profile is also supported by the morphology of the cross section shown in Fig. 3 in which silicon is seen in the FL as randomly distributed precipitates.

Based on the entire depth profile of the AR sample, it was possible to determine where the craters should be made to perform the local electrochemical measurements. Each crater was determined by the change in the slope shown in the depth profile. These results were essential in the choice of the sputtering times for the sample preparation (for the micro-cell analyses that are presented in the next section). Correlating Figs. 3 and 5 (b), it is possible to determine that the craters obtained for 50 s, 100 s and 250 s of sputtering are regarding the FL (Fig. 3 (c) - spectrum 1). Additionally, the crater obtained after 350 s of sputtering is related to the IDL; most likely to the UIDL (Fig. 3 (c) - spectrum 2). It is possible that there is some residual elementary contribution of the adjacent layer in the UIDL crater. Additionally, a deeper sputtering was made in order to obtain a crater in the steel substrate (not shown in Fig. 5). The position of the craters was confirmed by SEM analysis of their cross-section.

Fig. 6 shows the GDOES profiles for the PHS sample which were used as reference to determine where the craters should be made. The depth profile for the PHS sample, Fig. 6 (b), shows that the coating layer also has a thickness of around 25 μm. It is important to highlight that when the iron content increases (characterised by slight peaks in the iron profile - yellow line in Fig. 6 (b)) the amount of silicon also increases, while the aluminium content decreases (see line profiles in Fig. 6). Based on this, the different sublayers of the coating can be easily identified. Each crater determined in Fig. 6 can be correlated with the layers in Fig. 4.

The craters obtained after a sputtering for 70 s and 280 s reached the layers 1 and 3 which are Al-rich layers (see Fig. 4 - spectra 1 and 3). The crater after 140 s of sputtering is correlated to layer 2 which is Fe/Si-rich (Fig. 4 - spectrum 2); and the crater obtained at 400 s of sputtering is correlated to the IDL (Fe-rich layer). Although Fig. 4 (b) - spectrum 6 shows that the IDL consists of a low silicon content (1.3 % in mass fraction), the GDOES depth profile shows that the crater obtained after 300 s of sputtering presents a high silicon content (about 10 % in mass fraction). Thus, it was established that the crater made in the IDL corresponds to the region with voids in the top section of the IDL (see Fig. 4 (a)), because at this position the silicon content is higher as suggested by the EDS mapping in Fig. 4 (c). In addition to the craters made in the coating layer, two extra craters were made in order to reach the steel substrate at 500 s and 1000s of sputtering (not shown in Fig. 6). As already mentioned, the position of the craters was also confirmed by their cross-section SEM analyses.

3.3. *Local anodic potentiodynamic polarisation using electrochemical micro cell as a function of depth*

Representative anodic potentiodynamic polarisation curves obtained in the craters made at different positions of the coating layer, on the steel substrate and on the surface of the sample for the AR material are shown in Fig. 7. These individual curves were selected out of the several measurements for each position (at least three). They are not average curves, but they do show the important electrochemical trends. Table 2 shows the average values of corrosion potential (E^*), the breakdown potential (E_{BD}) and their corresponding standard deviations.

As can be seen in Fig. 7, except for the substrate, the shape of all the curves is very similar. A passive behaviour is seen in all of them and a sudden increase of the current is observed at a potential, known as the breakdown potential (E_{BD}), specific for each curve, which represent the

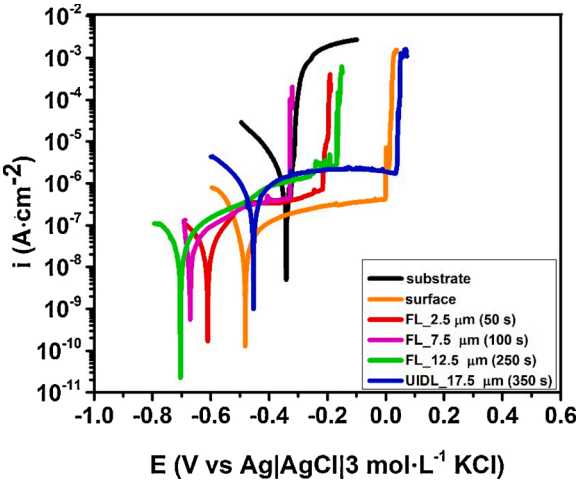

Fig. 7. Anodic potentiodynamic polarisation curves in 0.1 mol·L^{-1} NaCl solution acquired by means of electrochemical micro-cell as a function of the depth and also at the surface for as received 22MnB5 steel coated with hot-dip Al-Si (10 % Si in mass fraction).

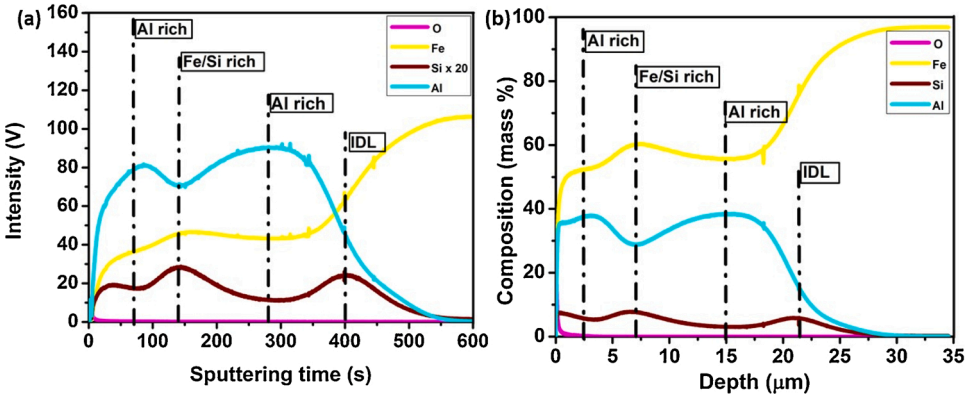

Fig. 6. GDOES profiles for press-hardened 22MnB5 steel coated with hot-dip Al-Si. (a) sputtering time profile showing by dashed lines the craters obtained after 70 s, 140 s, 280 s and 400 s of sputtering; (b) depth profile showing the craters obtained as a function of their depth and elemental chemical composition for Al, Si, Fe and O.

Table 2
Average E*, E_{BD}, and their corresponding standard deviations, determined from anodic potentiodynamic polarisation curves in 0.1 mol·L^{-1} NaCl at the surface and different depths in the AR sample.

AR sample	E^* (V vs Ag|AgCl|KCl sat.)		E_{BD} (V vs Ag|AgCl|KCl sat.)	
	Average	Standard deviation	Average	Standard deviation
Surface	−0.46	0.02	0.002	0.012
FL_2.5 μm	−0.59	0.03	−0.192	0.054
FL_7.5 μm	−0.62	0.05	−0.364	0.033
FL_12.5 μm	−0.70	0.02	−0.205	0.035
UIDL_17.5 μm	−0.42	0.04	0.022	0.028
Steel substrate [a]	−0.36	0.08	–	–

[a] ferrite/pearlite microstructure.

breakdown of the passive film [19]. On the contrary, the substrate anodic potentiodynamic polarisation curve shows an active behaviour, characteristic of carbon steel in chloride media [19].

The passive behaviour of the coating layers is characteristic of Al-based alloys [40,41]. Additionally, De Graeve et al. [19] have reported that after sputtering by GDOES an oxide layer might be formed in the bottom of the craters which support the passive behaviour of the curves shown in Fig. 7. The UIDL has the highest average E_{BD} (0.022 V vs Ag|AgCl|KCl sat.) followed by the surface's average E_{BD} (0.002 V vs Ag|AgCl|KCl sat.). The FL E_{BD} values show a variation without a trend as a function of depth.

According to Fig. 7 and Table 2, the surface presents higher average E^* (-0.46 V vs Ag|AgCl|KCl sat.) than the three underlying FL which present low values independent of the depth. The difference between the average corrosion potentials (ΔE^*) of the three curves in the FL is small; the highest ΔE^* value is around 0.11 V (FL at 12.5 μm and FL at 2.5 μm). As the less noble layer, the FL layers could provide cathodic protection to its adjacent UIDL; especially the FL at 12.5 μm which presents the lowest value of E^*. The steel substrate shows the noblest average E^* (-0.36 V vs Ag|AgCl|KCl sat.). Therefore, the whole coating layer could provide cathodic protection to the steel substrate. However, the average potential difference between the UIDL and the steel substrate is only about 0.06 V, which is too low for the UIDL to behave as a sacrificial anode. This difference increases to 0.34 V if the comparison is made between the steel substrate and the FL at 12.5 μm. From this analysis, it is possible to establish the following galvanic series, considering the average values of E*: $E^*_{FL\_12.5\mu m} < E^*_{FL\_7.5\mu m} \approx E^*_{FL\_2.5\mu m} < E^*_{UIDL} < E^*_{surface} < E^*_{steel}$.

The qualitative analysis of the current density in the anodic branch (i_a) indicates that the surface and the FL display a lower i_a than the UIDL and the steel substrate. In particular, the steel substrate shows the highest i_a, indicating high corrosion susceptibility in 0.1 mol·L-1 NaCl solution.

Fig. 8 shows the most representative curves obtained by means of anodic potentiodynamic polarisation acquired at the surface and in the craters at different coating sublayers and in the steel substrate for the PHS. It is important to mention that, during the measurements, the Al-rich layers and the surface presented both passive and active behaviour. Even the steel substrate showed a small passivity in one of the measurements. On the other hand, the Fe/Si-rich layer and the IDL presented only passive behaviour. The curves of Fig. 8 were selected among the curves (at least three) obtained for each position. For the Al-rich layer, only curves presenting active behaviour were selected because of the influence of iron enrichment as discussed further. The average values of E^* and E_{BD}, as well as their standard deviation values are summarised in Table 3.

From Fig. 8, it can be seen that the hot-stamping process shifted the overall E^* of the coating layer towards nobler values. Moreover, the ΔE^* among the curves is very small. Based on Table 3, the average E^* of the surface increased around 0.16 V after the thermo-mechanical process. The average E^* values of the Al-rich layers are very similar to each other

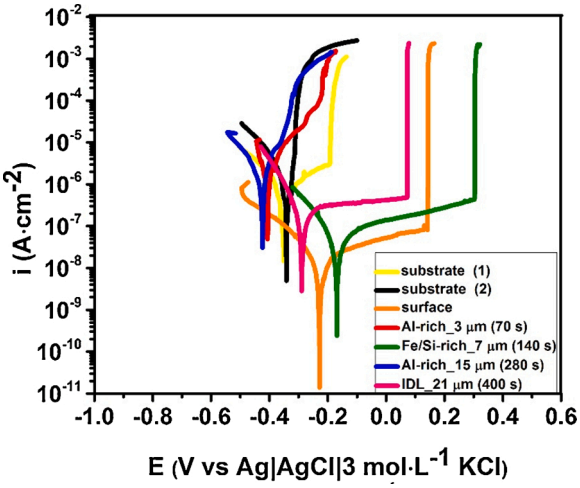

Fig. 8. Anodic potentiodynamic polarisation curves in 0.1 mol·L^{-1} NaCl solution acquired by means of electrochemical micro-cell in different positions of coating layer and steel substrate for as press-hardened 22MnB5 steel (PHS) coated with hot-dip Al-Si.

Table 3
Average E*, E_{BD}, and their standard deviation values, determined from anodic potentiodynamic polarisation curves in 0.1 mol·L^{-1} NaCl at the surface and different depths in the PHS sample.

PHS sample	E^* (V vs Ag|AgCl|KCl sat.)		E_{BD} (V vs Ag|AgCl|KCl sat.)	
	Average	Standard deviation	Average	Standard deviation
Surface	−0.30	0.08	0.165	0.334
Al-rich_3 μm	−0.40	0.05	0.149	0.120
Fe/Si-rich_7 μm	−0.23	0.06	0.270	0.181
Al-rich_15 μm	−0.41	0.08	0.104	0.072
IDL_21 μm	−0.32	0.03	0.148	0.075
Steel substrate [b]	−0.38	0.07		

[b] martensite microstructure.

(-0.40 V and -0.41 V Ag|AgCl|KCl sat.). Furthermore, they are lower than the Fe/Si rich layer (-0.23 V vs Ag|AgCl|KCl sat.) and very close to the IDL (-0.32 V vs Ag|AgCl|KCl sat.) and the substrate (-0.38 V vs Ag|AgCl|KCl sat.). Therefore, Al-rich sublayers could play the role of sacrificial anode for the Fe/Si-rich layer and the IDL, but not for the substrate. For the steel substrate the Al-rich layers can only protect by forming a barrier. Based on the average values of E^*, shown in Table 3, the following galvanic series is presented: $E^*_{Al\text{-}rich} < E^*_{steel} < E^*_{IDL} < E^*_{surface} < E^*_{Fe/Si\text{-}rich}$.

As already mentioned, the polarisation curves obtained from different samples in the Al-rich layers showed both passive and active behaviour. Moreover, the average E_{BD} of the curves with passive behaviour had a high standard deviation. These results suggest a high heterogeneity of the exposed area on which the curves were obtained. This fact can be ascribed to the lack of the flatness (see Fig. 4) and of the depth heterogeneity of the Al-rich sublayers. The latter was verified in previous studies [2,3,18].

Comparing Tables 2 and 3, it can be verified that after hot stamping there was a shift towards nobler values of all coating sublayers. The Fe/Si-rich layer has the highest average E_{BD} (0.270 V vs Ag|AgCl|KCl sat.), while the Al-rich layers have an average E_{BD} in the range from 0.104 V to 0.149 V vs Ag|AgCl|KCl sat.). Based on the average values, the E_{BD} sequence can be drawn as: $E_{BD\text{ - Al-rich}} \approx E_{BD\text{ - IDL}} < E_{BD\text{ - surface}} < E_{BD\text{ - Fe/Si-rich}}$. Concerning i_a, the qualitative analysis shows that the surface and the Fe/Si-rich layers presented the lowest i_a in the passive range of the polarisation curve. On the other hand, the Al-rich layers and the steel

substrate have the highest i_a indicating their high corrosion susceptibility in 0.1 mol·L^{-1} NaCl.

The results indicate that the hot-stamping process has a large influence on the electrochemical behaviour of the Al-Si coating. On the other hand, even though the steel substrate had changed its microstructure from pearlite-ferrite into martensite, due to the thermo-mechanical process, the electrochemical behaviour of the steel in terms of average E^* and i_a was not affected by the hot-stamping process.

4. Discussion

4.1. GDOES as a sample tool preparation

In general, it is possible and relatively simple to correlate the surface of the craters with the different sublayers in the coatings identified by FE-SEM / EDS analyses. However, one of the drawbacks of using GDOES as a sample preparation technique is the difficulty of sputtering the rough interfaces and exposing the entire surface of the thin sublayers [19,20,42]. Consequently, there will be an influence of other phases exposed together with the desired phase on the electrochemical results. This was probably the case for the crater in the UIDL for the AR sample, and the craters in the Al-rich sublayers and in the IDL for the PHS condition. The UIDL (AR) may also experience the influence of the LIDL which is very thin. This was further confirmed by the craters' cross-sections (not shown). However, a clear distinction / trend was obtained in the general electrochemical behaviour of the different sublayers analysed. It is important to highlight that the sputtering of the PHS sample sublayers was more difficult. This is due to the difference in hardness among the phases (layers) and the non-uniform morphology of the sublayers [2,18]. Another drawback can be related to the oxide layers on the bottom of the craters. As already mentioned, De Graeve et al. [19] have reported that the sputtering may lead the formation of oxide layer on the bottom of the craters. However, a thin oxide layer will always be present, mainly in the Al-rich sublayers, as the sputtering changes the surface characteristics. Therefore, a long interval between the procedure of making the crater by GDOES and carrying out the electrochemical measurements may cause the thickening of the oxide layer on the bottom of the craters.

4.2. Electrochemical depth profile of the 22MnB5 steel coated with hot-dip Al-Si (Si 10 % in mass fraction)

As shown in Fig. 7 and Table 2, the high average E^* of the outer surface is likely attributed to the native oxide layer which is characteristic of Al-based alloys [40]. This thin oxide layer contributes for the passive behaviour of the surface. If a damage occurs at the surface and exposes the coating, the FL could provide cathodic protection to the UIDL. Moreover, the E^* seems to decrease as a function of depth in the FL. However, a trend correlating E^* as a function of depth cannot be established because it is probably more related to the influence of the precipitates, as shown in Fig. 3 (a). The higher average E^* of the UIDL in comparison with the FL might be justified by the amount of silicon and iron present in it. According to the galvanic series, aluminium is less noble than iron and silicon [43]. However, the steel substrate showed the highest E^*. This suggests that the steel substrate could be protected by the coating by means of cathodic protection, but, as already mentioned, the driving force (the potential difference) may not be enough for the coating to corrode preferentially instead of the steel. The average ΔE^* between the UIDL and the steel substrate is only 0.06 V. Allély et al. [4] have pointed out that the minimum driving force necessary for providing cathodic protection is a potential difference of 0.05 V.

The predominance of the passive behaviour seen in Fig. 7 might also be related to the thickening of the oxide layer inside the craters made by means of GDOES. Nevertheless, this passive layer may breakdown from a specific potential for each sublayer (E_{BD}). The lower E_{BD} of the FL is related to the presence of precipitates which lead to the formation of a flawed oxide film and, thus, galvanic couples with the aluminium matrix [19,28]. As the precipitates act as cathodic sites, the surrounding aluminium matrix will start to corrode, promoting localised corrosion [19,35]. This was experimentally confirmed in our previous work, in which the same samples were evaluated by means of SKPFM technique [23]. The corrosion morphology of the specimens after immersion in NaCl solution (3.5 % in mass fraction) revealed that the attack in the AR samples was characterised by pitting corrosion initiated around the precipitates [23]. Conversely, the UIDL shows the higher E_{BD}, which is related to the homogeneity in terms of layer composition [19], consisting of iron and silicon.

The corrosion mechanism of the Al-Si (10 % Si in mass fraction) coating/steel substrate system, before hot stamping, can be summarised according Fig. 9. (I) The native oxide layer at the surface acts as a protective barrier and shows low i_a (II) In the case of damages at the native oxide layer the FL is exposed; its corrosion occurs localised around the precipitates. (III) If damage reaches the UIDL, the FL will be corroded preferentially behaving as a sacrificial anode to the UIDL as it presents the lowest average E^*. Moreover, the FL does have an i_a as low as the top oxide layer, which means that, despite it corrodes at low potential, its corrosion susceptibility (in 0.1 mol·L^{-1} NaCl) is also low. As long as the steel substrate is not exposed, the UIDL will protect the steel substrate by means of a barrier mechanism and not by cathodic protection because of the small potential difference among them. (IV) In case of steel exposure by severe damages in the coating, the steel substrate would corrode like the UIDL (in terms of corrosion potential) with a high corrosion rate due to its highest i_a indicating the high corrosion susceptibility of the steel substrate in this media (0.1 mol·L^{-1} NaCl). As the UIDL shows an i_a higher than the FL and the surface, it can be suggested that the corrosion susceptibility of the sublayers seems to be closely related to the amount of iron in them.

The electrochemical behaviour of Al-Si coatings has been evaluated before using the same approach of depth profiling. De Graeve et al. [19] evaluated the influence of silicon content by means of GDOES combined with electrochemical micro cell. The authors have shown, considering the E^*, that the FL would corrode preferentially compared to the steel substrate and the IDL, but the steel would be protected mainly by barrier mechanism provided by the IDL (as the IDL had higher E^* than the interstitial free steel). Additionally, they were able to investigate the electrochemical behaviour of the LIDL which presented the noblest value of E^*. Lemmens et al. [20] investigated the addition of 1 % of silicon (in mass fraction) in hot-dip aluminized steels using GDOES combined with scanning vibration electrode technique (SVET). The methodology employed has provided insights about the current distribution of the different coating sub layers in 0.05 mol·L^{-1} NaCl. In general, the authors pointed out that the FL presented a very low activity. However, the silicon addition promoted irregular anodic distribution in the FL which is attributed to the presence of precipitates. Conversely, cathodic currents were measured for the UIDL, LIDL and the steel substrate. The highest cathodic current was measured in the LIDL. These findings are in agreement with the work of Vu et al. [44] who have analysed the sacrificial behaviour in cut-edge steel coated with Al-Si exposed in chloride media by means of in situ current and pH measurements. The authors have shown that in chloride media the corrosion of the coating starts locally which results in both local activation and depassivation of the coating. Consequently, the coating behaves sacrificially versus the steel [44]. In the present study, a further step has been considered, the Al-Si system was submitted to a hot-stamping process, which greatly influences the structure and composition of the metallic coating and, therefore, the electrochemical relation between the different sublayers.

4.3. Influence of hot stamping on the electrochemical depth profile

Comparing the results from Figs. 7 and 8, the evaluation of the

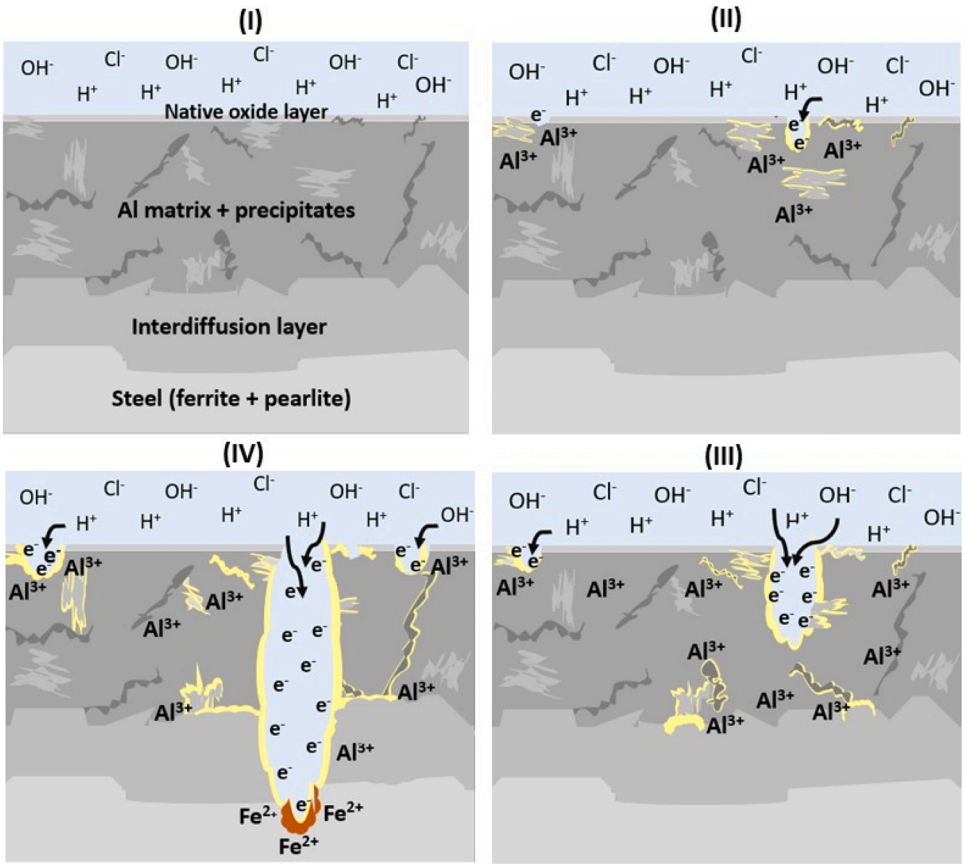

Fig. 9. Schematic diagram of the proposed corrosion mechanism for 22MnB5 steel coated with hot-dip Al-Si (Si 10 % in mass fraction) showing: (I) initial condition of the system, absent of defects at the surface in which the native oxide layer acts as a protective barrier; (II) damage at the surface and the beginning of the corrosion process of the coating matrix (free layer) localised around the precipitates; (III) damage reaches the interdiffusion layer and the coating matrix plays a role of sacrificial anode, corroding preferentially; (IV) the steel substrate is exposed and it corrodes similarly to the interdiffusion layer; moreover, the corrosion process of the coating matrix increases.

influence of the hot-stamping process on the corrosion mechanism was possible. The first highlight is regarding the overall shift of E^* and E_{BD} towards nobler values. These results are in agreement with a previous study which evaluated the effect of hot stamping using SKPFM [23]. An increase on the (Volta) potential of the coating layer was seen after hot stamping, as well as a minimal potential difference among the sublayers and a decrease in driving force for cathodic protection [23]. Although SKPFM and the electrochemical micro cell present different principles, the present investigation has indicated a similar trend among the coating's sublayers.

During hot stamping, iron diffuses from the steel substrate towards the coating. Thus, the whole coating layer becomes enriched in iron, and the coating presents a multi-layered structure. Even the surface becomes enriched in iron as shown in previous studies [4,9]. Allély et al. [4] have reported the presence of a mixture of oxides composed of iron, aluminium and silicon as corrosion products on the surface of PHS coated with Al-Si. The presence of iron and silicon on the surface might be the reason for the increase of the surface's E^*. Moreover, the oxide layer formed after hot stamping (thermal oxides) may be thicker than the native aluminium oxide layer, enhancing the passive behaviour and being the probable reason for a higher E_{BD}. As the average E^* of the surface (oxide layer) is higher than that of the Al-rich phases, the possible protection mechanism is only by barrier protection. Among all the sublayers in the coating, the Al-rich phases presented similar average E^* as the steel substrate (around -0.40 V vs Ag|AgCl|KCl sat.). This could be due to the high amount of iron found in these layers after hot stamping. These layers could provide some cathodic protection to the Fe/Si-rich layer, but there is just a small driving force for that (only 0.16 V). The Fe/Si-rich layer presents the noblest average E^* (-0.23 V vs Ag|AgCl|KCl sat.), though, it is only 0.09 V higher than the IDL.

The reason for the shift towards nobler potential values could be related to the silicon influence. According to the depth profile presented in Fig. 6, the silicon content is relatively higher in the Fe/Si-rich layer than in the IDL. The presence of silicon might be also the reason for the highest E_{BD} of the Fe/Si-rich layer. As the precipitates are no longer seen in the PHS condition, the overall E_{BD} shifted towards more positive values for those curves presenting a passive behaviour. Previous studies have found that the addition of silicon in steel leads to the decrease of iron oxidation rate at high temperatures [45]. This mechanism is related to the formation of a silicon oxide at the surface which inhibits the diffusion of iron throughout the surface, consequently avoiding its oxidation [45]. This effect could be related to the passivation of the sublayers presenting a high silicon content in PHS (Fe/Si-rich layers). However, further and dedicated research is necessary in order to fully understand the effect of Si in the passivity of these Fe-Si intermetallic phases.

The hot stamping changed the electrochemical behaviour of the coating layer but did not change the electrochemical behaviour of the steel substrate even considering the microstructure transformation from pearlite-ferrite to martensite. Although one of the curves regarding the steel substrate for PHS sample shows a small passivity range, this behaviour is not a trend. However, it is an important observation since this is mostly related to the thickening of the oxide layer on the bottom of the crater. In a previous study, using the SKPFM local technique, the authors have noticed that the Volta potential of the steel substrate is slightly shifted to nobler values after hot stamping [23]. The martensite transformation is a known process to provoke residual stress on the material, and the Volta potential is very sensitive to any change in the sample surface [46]. The effect of phase transformation on the steel substrate should be more pronounced in terms of Volta-potential difference than any other potential measured by means of conventional electrochemical techniques (e.g. corrosion potential) [23].

As already mentioned, during the micro-cell measurements, the Al-rich layers and the surface presented both passive and active

behaviour. The probable reason for the active behaviour of the Al-rich phases could be the iron enrichment which is around 45 % (in mass fraction), as seen in Fig. 4(b) spectra 1 and 3. The iron enrichment can also be the reason why the Al-rich layers presented the highest i_a, similar to the steel substrate. Conversely, for the curves showing passive behaviour during the measurements, it could be because of the thickening of oxides on the bottom of the craters in the Al-rich sublayers, due to the different intervals between making the crater by GDOES and carrying out the electrochemical measurements. Another hypothesis for the active behaviour of the Al-rich phases as well as the surface could be the presence of micro cracks. On the contrary, during the micro-cell measurements, the acquired curves for the IDL and the Fe/Si-rich layer showed only passive behaviour. Despite the open discussion about the most appropriate stoichiometry for each sublayer in PHS coated with Al-Si, there is a consensus that the Al-rich layers are harder and brittle whereas the Fe/Si-rich layers and the IDL are more ductile [18,23,24,47]. This might contribute to the density of cracks as well as their formation and propagation. Fan et al. [18] have shown that the cracks initiate from the surface and they are limited at the IDL. The authors have pointed out two reasons for the formation and propagation of cracks: the thermal expansion and the difference on mechanical properties between the sublayers. Therefore, the initial cracks do not reach the steel substrate as the IDL has a similar thermal expansion coefficient to the steel substrate, due to the high iron content in its composition [24]. Furthermore, the predominant passive behaviour and the enhancement of the E_{BD} of the Fe/Si-rich layer and the IDL could be attributed to the presence of silicon.

Concerning the i_a either for AR and PHS samples, they show low order of magnitude from 10^{-8} A cm^{-2} to 10^{-6} A cm^{-2}. These are expected current density ranges for curves presenting a passive behaviour. However, for those curves where the active behaviour is predominant, a higher order of magnitude would be expected, such as 10^{-5} A cm^{-2}. The latter corresponds to the limiting current density of the oxygen which determines the Fe and also Al corrosion rate in aerated solution [48]. Thus, the relatively low order of magnitude of i_a for those curves presenting active behaviour (10^{-6} A cm^{-2}) could be another indication of the influence of the oxide layer on the bottom of the craters.

From the results presented, the following protection mechanism for coated PHS, considering the 0.1 mol·L^{-1} NaCl as an electrolyte is proposed in Fig. 10. (I) Damages (cracks) are already seen from the surface throughout the whole coating layer. The surface consists of a thermal oxide layer thicker than the native oxide layer from the AR condition. (II) The presence of damages enhances the corrosion process: the oxide layer at the surface acts as a protective barrier to the Al-rich layer; the surface will corrode at relatively high potentials, exhibiting low i_a. The Al-rich layer, independent of the depth, could play the role of sacrificial anode for the Fe/Si-rich and/or the IDL, corroding preferentially and exhibiting high corrosion rates. Finally, the steel substrate will be protected by only barrier mechanism. (III) In case of severe damage and the exposure of the steel substrate, the latter will corrode as much as the Al-rich layers due to their similar E^* and i_a.

5. Conclusion

The effect of the hot-stamping process on the electrochemical behaviour was systematically evaluated using a depth profiling approach combining GDOES and an electrochemical micro cell. The main findings are summarised as follows:

i After hot stamping, the coating becomes a multi-layered structure highly influenced mostly by iron diffusion into the coating. The iron

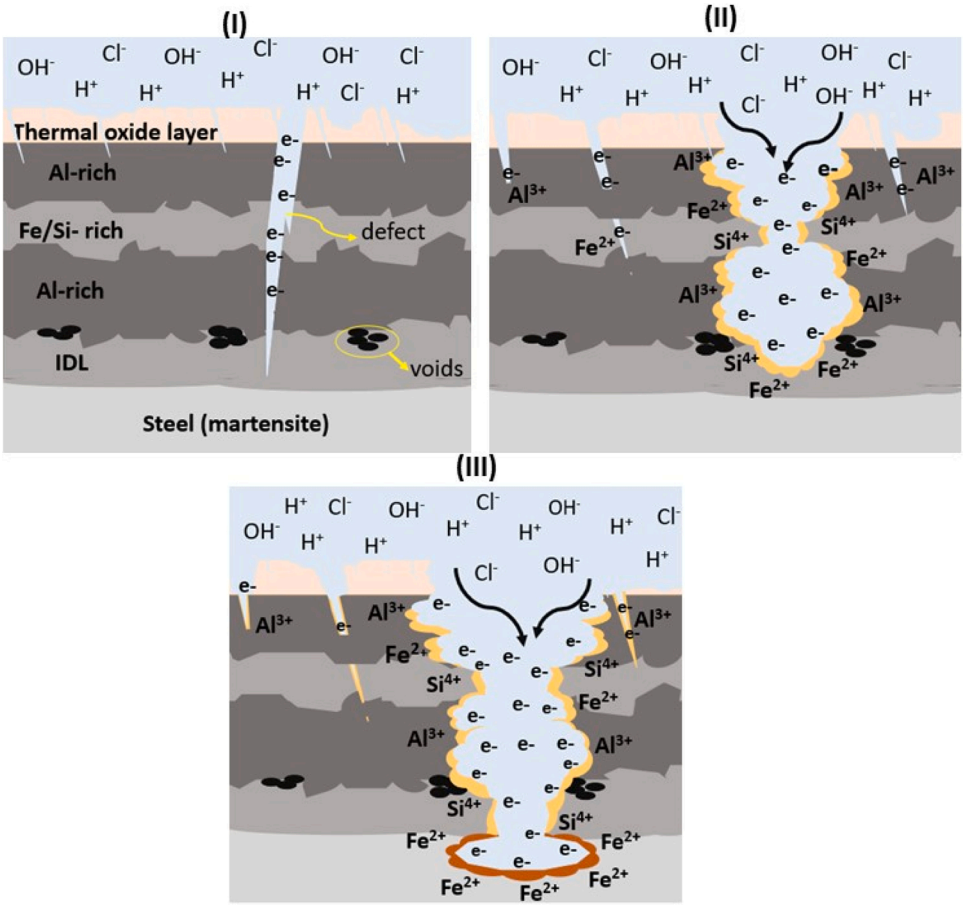

Fig. 10. Schematic diagram showing the proposed corrosion mechanism for press-hardened 22MnB5 steel coated with hot-dip Al-Si from: (I) initial condition of the system which already shows several damages at the surface and in the coating layer; (II) as the oxide layer plays a role of protective barrier, the coating sublayers start to corrode, but the corrosion of the Al-rich sublayers is more pronounced as they could behave as sacrificial anode to the Fe/Si-rich layer and the IDL; (III) the coating layer provides a barrier protection to the steel substrate; when it is exposed it corrodes as much as the Al-rich sublayers due to their similar corrosion potential and corrosion rate.

enrichment is the reason for the overall increase of corrosion potential of the coating layer.

ii The increased potential of the surface is attributed to the formation of an oxide layer (thermal oxides), thicker than the native aluminium oxide layer, probably containing also silicon and iron oxides.

iii Silicon precipitates are no longer seen after hot stamping. The presence of silicon in solid solution was attributed as the reason for the predominant passive behaviour of the Fe/Si-rich layer and the IDL. Moreover, the high silicon content in the Fe/Si-rich layer has been indicated as the reason for its highest corrosion and breakdown potential.

iv The predominant active behaviour of the Al-rich layers was mainly related to the iron enrichment. Whereas the passive behaviour can be attributed to the formation of an oxide layer on the bottom of the craters made by GDOES. The presence of micro cracks may also affect the electrochemical behaviour of both the Al-rich phases and the surface.

v The hot-stamping process did not change the electrochemical behaviour of the steel substrate. However, it did change the electrochemical behaviour of the coating layer, which became nobler. Thus, after hot stamping the steel can be protected only by barrier protection.

Data availability

The raw/processed data required to reproduce these findings cannot be shared at this time as the data also forms part of an on-going study.

CRediT authorship contribution statement

Camila Pucci Couto: Conceptualization, Writing - original draft, Writing - review & editing, Visualization. **Francesco Andreatta:** Methodology, Validation, Writing - review & editing. **Alex Lanzutti:** Methodology, Validation, Writing - review & editing. **Isolda Costa:** Writing - review & editing. **Zehbour Panossian:** Writing - review & editing. **Iris De Graeve:** Validation, Writing - review & editing. **Herman Terryn:** Methodology, Validation, Writing - review & editing, Supervision. **Jesualdo Luiz Rossi:** Validation, Writing - review & editing, Visualization, Supervision. **Reynier I. Revilla:** Conceptualization, Validation, Writing - review & editing, Visualization, Supervision.

Declaration of Competing Interest

The authors declare no conflict of interest.

Acknowledgments

The authors would like to thank the Brazilian Coordination for Higher Education (CAPES), process 88881.189691/2018-01, and the Brazilian National Council for Scientific and Technological Development (CNPq), process 205368/2018-2, for the scholarship granted to Camila Pucci Couto. In addition, the authors would like to thank Bart Lippens, for the samples cross-section preparation, and Priya Laha, for her assistance with the FE-SEM-EDS. Finally, the authors thank the companies General Motors Mercosul and ArcelorMittal, for materials' supply.

References

[1] H. Karbasian, A.E. Tekkaya, A review on hot stamping, J. Mater. Process. Technol. 210 (2010) 2103–2118, https://doi.org/10.1016/j.jmatprotec.2010.07.019.

[2] M. Windmann, A. Röttger, W. Theisen, Phase formation at the interface between a boron alloyed steel substrate and an Al-rich coating, Surf. Coatings Technol. 226 (2013) 130–139, https://doi.org/10.1016/j.surfcoat.2013.03.045.

[3] M. Windmann, A. Röttger, W. Theisen, Formation of intermetallic phases in Al-coated hot-stamped 22MnB5 sheets in terms of coating thickness and Si content, Surf. Coatings Technol. 246 (2014) 17–25, https://doi.org/10.1016/j.surfcoat.2014.02.056.

[4] C. Allély, L. Dosdat, O. Clauzeau, K. Ogle, P. Volovitch, Anticorrosion mechanisms of aluminized steel for hot stamping, Surf. Coatings Technol. 238 (2014) 188–196, https://doi.org/10.1016/j.surfcoat.2013.10.072.

[5] G. Venturato, M. Novella, S. Bruschi, A. Ghiotti, R. Shivpuri, Effects of phase transformation in hot stamping of 22MnB5 high strength steel, Proced. Eng. 183 (2017) 316–321, https://doi.org/10.1016/j.proeng.2017.04.045.

[6] K. Mori, P.F. Bariani, B.-A. Behrens, A. Brosius, S. Bruschi, T. Maeno, M. Merklein, J. Yanagimoto, Hot stamping of ultra-high strength steel parts, CIRP Ann. 66 (2017) 755–777, https://doi.org/10.1016/j.cirp.2017.05.007.

[7] Y. Nakagawa, K.I. Mori, S. Yashima, T. Kaido, Springback behaviour and quenchability in hot stamping of thick sheets, Proced. Manuf. 15 (2018) 1071–1078, https://doi.org/10.1016/j.promfg.2018.07.385.

[8] M. Merklein, J. Lechler, Investigation of the thermo-mechanical properties of hot stamping steels, J. Mater. Process. Technol. 177 (2006) 452–455, https://doi.org/10.1016/j.jmatprotec.2006.03.233.

[9] L. Dosdat, J. Petitjean, T. Vietoris, O. Clauzeau, Corrosion resistance of different metallic coatings on press-hardened steels for automotive, Steel Res. Int. 82 (2011) 726–733, https://doi.org/10.1002/srin.201000291.

[10] J. Kondratiuk, P. Kuhn, E. Labrenz, C. Bischoff, Zinc coatings for hot sheet metal forming: comparison of phase evolution and microstructure during heat treatment, Surf. Coatings Technol. 205 (2011) 4141–4153, https://doi.org/10.1016/j.surfcoat.2011.03.002.

[11] R. Neugebauer, F. Schieck, S. Polster, A. Mosel, A. Rautenstrauch, J. Schönherr, N. Pierschel, Press hardening - an innovative and challenging technology, Arch. Civ. Mech. Eng. 12 (2012) 113–118, https://doi.org/10.1016/j.acme.2012.04.013.

[12] D.W. Fan, H.S. Kim, S. Birosca, B.C. De Cooman, Critical review of hot stamping technology for automotive steels, Mater. Sci. Technol. (2007) 99–110.

[13] R. Autengruber, G. Luckeneder, A.W. Hassel, Corrosion of press-hardened galvanized steel, Corros. Sci. 63 (2012) 12–19, https://doi.org/10.1016/j.corsci.2012.04.048.

[14] M. Windmann, A. Röttger, I. Hahn, W. Theisen, Mechanical properties of AlXFeY intermetallics in Al-base coatings on steel 22MnB5 and resulting wear mechanisms at press-hardening tool steel surfaces, Surf. Coatings Technol. 321 (2017) 321–327, https://doi.org/10.1016/j.surfcoat.2017.04.075.

[15] H. Järvinen, M. Isakov, T. Nyyssönen, M. Järvenpää, P. Peura, The effect of initial microstructure on the final properties of press hardened 22MnB5 steels, Mater. Sci. Eng. A. 676 (2016) 109–120, https://doi.org/10.1016/j.msea.2016.08.096.

[16] H. Järvinen, M. Honkanen, M. Patnamsetty, S. Järn, E. Heinonen, H. Jiang, P. Peura, Press hardening of zinc-coated boron steels: role of steel composition in the development of phase structures within coating and interface regions, Surf. Coatings Technol. 352 (2018) 378–391, https://doi.org/10.1016/j.surfcoat.2018.08.040.

[17] D.W. Fan, B.C. De Cooman, State-of-the-knowledge on coating systems for hot stamped parts, Steel Res. Int. 83 (2012) 412–433, https://doi.org/10.1002/srin.201100292.

[18] D.W. Fan, H.S. Kim, J.-K. Oh, K.-G. Chin, B.C. De Cooman, Coating degradation in hot press forming, ISIJ Int. 50 (2010) 561–568, https://doi.org/10.2355/isijinternational.50.561.

[19] I. De Graeve, I. Schoukens, A. Lanzutti, F. Andreatta, A. Alvarez-Pampliega, J. De Strycker, L. Fedrizzi, H. Terryn, Mechanism of corrosion protection of hot-dip aluminium-silicon coatings on steel studied by electrochemical depth profiling, Corros. Sci. 76 (2013) 325–336, https://doi.org/10.1016/j.corsci.2013.07.005.

[20] B. Lemmens, Y. Gonzalez Garcia, B. Corlu, J. De Strycker, I. De Graeve, K. Verbeken, Study of the electrochemical behaviour of aluminized steel, Surf. Coatings Technol. 260 (2014) 34–38, https://doi.org/10.1016/j.surfcoat.2014.06.064.

[21] B. Lemmens, H. Springer, I. De Graeve, J. De Strycker, D. Raabe, K. Verbeken, Effect of silicon on the microstructure and growth kinetics of intermetallic phases formed during hot-dip aluminizing of ferritic steel, Surf. Coatings Technol. 319 (2017) 104–109, https://doi.org/10.1016/j.surfcoat.2017.03.040.

[22] W.J. Cheng, C.J. Wang, Microstructural evolution of intermetallic layer in hot-dipped aluminide mild steel with silicon addition, Surf. Coatings Technol. 205 (2011) 4726–4731, https://doi.org/10.1016/j.surfcoat.2011.04.061.

[23] C.P. Couto, R.I. Revilla, M.A. Colosio, I. Costa, Z. Panossian, I. De Graeve, H. Terryn, J.L. Rossi, Electrochemical behaviour of 22MnB5 steel coated with hot-dip Al-Si before and after hot-stamping process investigated by means of scanning Kelvin probe microscopy, Corros. Sci. 174 (2020), 108811, https://doi.org/10.1016/j.corsci.2020.108811.

[24] Z.-X. Gui, K. Wang, Y.-S. Zhang, B. Zhu, Cracking and interfacial debonding of the Al–Si coating in hot stamping of pre-coated boron steel, Appl. Surf. Sci. 316 (2014) 595–603, https://doi.org/10.1016/j.apsusc.2014.08.043.

[25] I. Yakubtsov, R. Sohmshetty, Evolution of Al-Si coating microstructure during heat-treatment of usibor ® 1500, IOP Conf. Ser. Mater. Sci. Eng. 418 (2018), 012015, https://doi.org/10.1088/1757-899X/418/1/012015.

[26] W. Yang, E. Hwang, H. Kim, S. Ahn, S. Kim, H. Castaneda, A study of annealing time to surface characteristics and hydrogen embrittlement on AlSi coated 22MnB5 during hot stamping process, Surf. Coatings Technol. 378 (2019), 124911, https://doi.org/10.1016/j.surfcoat.2019.124911.

[27] F. Andreatta, M.M. Lohrengel, H. Terryn, J.H.W. de Wit, Electrochemical characterisation of aluminium AA7075-T6 and solution heat treated AA7075 using a micro-capillary cell, Electrochim. Acta 48 (2003) 3239–3247, https://doi.org/10.1016/S0013-4686(03)00379-7.

[28] G. Buytaert, Premendra, J.H. Wde Wit, L. Katgerman, B. Kernig, H.J. Brinkman, H. Terryn, Electrochemical investigation of rolled-in subsurface layers in commercially pure aluminium alloys with the micro-capillary cell technique, Surf.

Coatings Technol. 201 (2007) 4553–4560, https://doi.org/10.1016/j.surfcoat.2006.09.096.
[29] A. Alvarez-Pampliega, Y. González-García, K. Van den Bergh, J. De Strycker, H. Terryn, Scanning Kelvin force microscopy study at the cut-edge of aluminum rich metal coated steel, Mater. Corros. 66 (2015) 16–22, https://doi.org/10.1002/maco.201307145.
[30] F. Andreatta, L. Fedrizzi, The use of the electrochemical micro-cell for the investigation of corrosion phenomena, Electrochim. Acta 203 (2016) 337–349, https://doi.org/10.1016/j.electacta.2016.01.099.
[31] H. Böhni, T. Suter, F. Assi, Micro-electrochemical techniques for studies of localized processes on metal surfaces in the nanometer range, Surf. Coatings Technol. 130 (2000) 80–86, https://doi.org/10.1016/S0257-8972(00)00681-2.
[32] T. Suter, H. Böhni, A new microelectrochemical method to study pit initiation on stainless steels, Electrochim. Acta 42 (1997) 3275–3280, https://doi.org/10.1016/S0013-4686(70)01783-8.
[33] F. Andreatta, H. Terryn, J.H. de Wit, Corrosion behaviour of different tempers of AA7075 aluminium alloy, Electrochim. Acta 49 (2004) 2851–2862, https://doi.org/10.1016/j.electacta.2004.01.046.
[34] T. Suter, H. Böhni, Microelectrodes for corrosion studies in microsystems, Electrochim. Acta 47 (2001) 191–199, https://doi.org/10.1016/S0013-4686(01)00551-5.
[35] F.N. Afshar, R. Ambat, C. Kwakernaak, J.H.W. De Wit, J.M.C. Mol, H. Terryn, Electrochemical depth profiling of multilayer metallic structures: an aluminum brazing sheet, Electrochim. Acta 77 (2012) 285–293, https://doi.org/10.1016/j.electacta.2012.06.023.
[36] Arcellor Mittal, Steels for hot stamping -Usibor® and Ductibor®, 10 (n.d.) 2226–2231. https://automotive.arcelormittal.com/products/flat/PHS/usibor_ductibo.
[37] A. Worldwide, Steels coated with Alusi ® aluminum- silicon alloy : specific applications, (n.d.).
[38] W.-J.J. Cheng, C.-J.J. Wang, Growth of intermetallic layer in the aluminide mild steel during hot-dipping, Surf. Coatings Technol. 204 (2009) 824–828, https://doi.org/10.1016/j.surfcoat.2009.09.061.
[39] A. Van Alboom, B. Lemmens, B. Breitbach, E. De Grave, S. Cottenier, K. Verbeken, Multi-method identification and characterization of the intermetallic surface layers of hot-dip Al-coated steel: FeAl3 or Fe4Al13 and Fe2Al5 or Fe2Al5+x, Surf. Coatings Technol. 324 (2017) 419–428, https://doi.org/10.1016/J.SURFCOAT.2017.05.091.
[40] N.L. Sukiman, X. Zhou, N. Birbilis, A.E. Hughes, J.M.C. Mol, S.J. Garcia, X. Zhou, G.E. Thompson, Durability and corrosion of aluminium and its alloys: overview, property space, techniques and developments. Alum. Alloy. - New Trends Fabr. Appl., InTech, 2012, https://doi.org/10.5772/53752.
[41] R.I. Revilla, H. Terryn, I. De Graeve, On the use of SKPFM for in situ studies of the repassivation of the native oxide film on aluminium in air, Electrochem. commun. 93 (2018) 162–165, https://doi.org/10.1016/j.elecom.2018.07.010.
[42] T. Nelis, R. Payling, N.W. Barneet, Qualitative depth profiling, in: T. Nelis, R. Payling, N.W. Barneet (Eds.), Glow Disch. Opt. Emiss. Spectrosc., 2003, pp. 123–135, https://doi.org/10.1039/9781847550989-00123.
[43] V. Gentil, Corrosão, 3rd ed., LTC, Rio de Janeiro, 1996.
[44] A.Q. Vu, B. Vuillemin, R. Oltra, C. Allély, In situ investigation of sacrificial behaviour of hot dipped AlSi coating in sulphate and chloride solutions, Corros. Sci. 70 (2013) 112–118, https://doi.org/10.1016/j.corsci.2013.01.018.
[45] A.R. Lashin, O. Schneeweiss, Y. Houbaert, Effect of ambient air pressure on the oxidation kinetics of Fe-6 at.% Si alloy, Corros. Sci. 50 (2008) 2580–2587, https://doi.org/10.1016/j.corsci.2008.06.036.
[46] C. Örnek, D.L.L. Engelberg, SKPFM measured Volta potential correlated with strain localisation in microstructure to understand corrosion susceptibility of cold-rolled grade 2205 duplex stainless steel, Corros. Sci. 99 (2015) 164–171, https://doi.org/10.1016/j.corsci.2015.06.035.
[47] Z. Gui, W. Liang, Y. Liu, Y. Zhang, Thermo-mechanical behavior of the Al–Si alloy coated hot stamping boron steel, Mater. Des. 60 (2014) 26–33, https://doi.org/10.1016/J.MATDES.2014.03.011.
[48] Z. Panossian, C.A.L. dos Santos, J.L. Cardoso, L.N. da Silva, R.A. Camargo, Interpretação De Curvas De Polarização (in Portuguese), ABRACO, ABRACO, Fortaleza/CE, 2014, pp. 1–28.